PROBABILISTIC ANALYSIS OF THERMAL LASER WEAPON SUBSYSTEM IN ANTI-DRONE SYSTEMS

Dharmaraja Selvamuthu[a], Utkarsh Dubey[a],
Raina Raj[b], Priyanka Kalita[c]

•

Department of Mathematics, Indian Institute of Technology Delhi, New Delhi, India[a]
dharmar@maths.iitd.ac.in
Utkarsh.mt613@maths.iitd.ac.in
Bharti School of Telecommunication Technology & Management,
Indian Institute of Technology Delhi, New Delhi, India[b]
rainaraj.curaj@gmail.com
Department of Statistics, Bhattadev University, Bajali, Pathsala - 781325, Assam, India[c]
priya.24723@gmail.com

Abstract

The rise of drones has introduced significant security threats, including unauthorized surveillance and explosive payloads. Drones threaten armies by enabling enemy surveillance, facilitating precision strikes on troops or equipment, disrupting communications, and introducing challenges in air defense, thereby altering traditional battlefield dynamics and strategies. To counter these threats, high-energy laser weapon subsystems provide precise, scalable responses with minimal collateral damage. This paper presents a probabilistic analysis of thermal laser subsystem's effects on targets, accounting for aiming and tracking errors. Atmospheric turbulence is modeled using the power spectrum inversion method, while Monte Carlo simulations calculate the on-target spot area. The energy distribution is converted to temperature using thermal physics, and the damage probability is determined by integrating temperatures exceeding material-specific thresholds. Simulation results confirm the system's effectiveness and reliability of thermal laser weapon systems in neutralizing aerial threats.

Keywords: Atmospheric Turbulence, Monte Carlo Simulation, Gaussian Beam, Laser Beam Propagation, Power Spectrum Inversion.

1. INTRODUCTION

Nowdays, drones have become readily available, affordable, and simple to operate, making them popular for parcel deliveries, film shoots, disaster surveillance, and even as a hobby for many. However, beyond these recreational uses and benefits, drones are sometimes misused for trespassing and spying on private properties using built-in cameras. In response to these threats, many have developed anti-drone systems designed to secure specific areas. These systems can detect and classify unauthorized drones and, in some cases, jam the signals used by controllers to operate the drones.

An anti-drone laser system is a crucial security technology designed to detect, track, and neutralize unauthorized drones operating in restricted airspace. These systems leverage advanced detection, precise tracking, and effective neutralization techniques to safeguard sensitive areas from potential drone threats. Laser weapons are rapidly emerging as an efficient solution to

DOI: https://doi.org/10.24412/1932-2321-2025-489-1213-1228

counter the increasing drone threat, offering light-speed engagement, pinpoint accuracy, and cost-effectiveness per shot [5]. To assess the effectiveness of lasers on drone engines, a comprehensive method for evaluating target vulnerability to laser strikes is studied in [3]. Ball, in [7], compared the assessment of laser vulnerability to evaluate the damage caused by non-explosive penetrating objects, though a detailed methodology was not provided.

Currently, many anti-drone systems utilize military-grade components to ensure the destruction of hostile drones. Military strategies often incorporate jamming systems to disrupt a drone's control channels [10]. Another key technology for drone neutralization is the laser power transmitter, which plays a pivotal role in preventing unauthorized drones from threatening critical infrastructure, military bases, and public events. Laser-based anti-drone systems use directed energy technology to disable or destroy hostile drones by focusing high-energy laser beams. In [2], Huang et al. developed a laser-integrated anti-drone system that combines advanced laser technology with sensors, tracking mechanisms, and command-and-control interfaces, offering a comprehensive defense against drone threats.

The key components and capabilities of a laser-integrated anti-drone system include:

High-Energy Laser Weapons: High-energy laser weapons are highly effective for neutralizing drone threats, offering precise and scalable effects with minimal collateral damage, unlike traditional projectile weapons [13]. Lyu and Zhan provided a comprehensive global overview of high-energy laser weapon technology in [4], highlighting its growing military use in safeguarding nations. The review covers the strategic and tactical roles of these systems on the battlefield, examining performance limitations such as laser device types, beam control systems, atmospheric propagation, and targeting effectiveness [6].

Detection System: Laser-integrated anti-drone systems feature advanced sensor suites, including radar, electro-optical/infrared cameras, and RF detectors, which provide enhanced situational awareness. These sensors work together to detect, track, and classify drones with precision, minimizing false alarms. Abunada et al. discussed an RF-based drone detection method in [1], while Wang et al. [12] explored the challenges of radar detection for small drones and proposed future improvement. Lasers can also complement other sensors by detecting, dazzling, or destroying a drone's optical sensors [8].

Tracking System: The tracking and targeting system is essential for accurately following drone movements and maintaining a lock on targets during engagement. This system uses advanced algorithms and predictive models to account for target motion, atmospheric conditions, and platform dynamics, ensuring precise laser beam placement. Steinvall [8] examined the effects of atmospheric conditions and tracking errors on laser performance as a sensor, countermeasure, or weapon.

Control Unit: The control unit of a laser-integrated anti-drone system offers a user-friendly interface for monitoring system status, analyzing threats, and executing engagement protocols. It provides real-time feedback on tracking, laser engagement, and overall performance, enabling operators to make informed decisions and adjust tactics as needed. In [1], Abunada et al. proposed an RF jamming system to disconnect drones from their controllers.

To date, no studies have been documented on the probabilistic analysis of an anti-drone laser system. This gap in the literature motivates our research to explore this area. The proposed work is the first to conduct a probabilistic analysis of an anti-drone laser system.

1.1. Contribution

This study presents a comprehensive probabilistic analysis of a thermal laser weapon system aimed at neutralizing aerial threats like drones. A probabilistic model was developed to account for atmospheric turbulence effects on laser propagation, the distribution of energy on the target, and the thermal response of the target material. By employing statistical methods and Monte Carlo simulations, complex interactions were simplified, allowing for the calculation of the probability of damage from sustained laser exposure. The peformance analysis considered the Gaussian profile of the laser beam, atmospheric phase screens, and the impact of aiming and

tracking errors. The Monte Carlo method provided a reliable approach to estimating the on-target spot area, which was essential for determining the energy distribution on the target. This energy distribution was then used to generate a temperature profile to evaluate thermal damage. Simulation results revealed that the effectiveness of the thermal laser weapon system is heavily influenced by atmospheric conditions, system accuracy, and the material properties of the target. Understanding these factors is critical for improving the precision and reliability of laser weapon systems in operational environments.

To summarize this article, the potential probabilistic model is described in Section 2, followed by the simulation results in Section 3. The case study is presented in Section 4, while Section 5 provides all the pseudo codes. Finally, Section 6 concludes with suggestions for further research.

2. SETTING UP THE MODEL

In traditional weapon systems, the probability of damage is determined by the probability of hitting the target ($P(\text{hit})$) multiplied by the probability that the damage exceeds the target's threshold strength: $P(\text{damage}) = P(\text{hit}) \cdot P(\text{damage} > \text{threshold})$. In contrast, damage probability is based on sustained thermal effects in laser systems. If $p(T)$ represents the temperature distribution of the target and T_D is the threshold temperature, then

$$P(\text{damage}) = \int_{T_D}^{\infty} p(T)\, dT. \tag{1}$$

This integral captures the cumulative probability that the target's temperature exceeds T_D, resulting in damage. The threshold temperature is assumed to be around the melting point of the target material and so, our aim is to find out the function $p(T)$. In the Celsius scale, this temperature is generally positive for metals.

The laser output arrives at the target after traversing a medium influenced by atmospheric turbulence. This turbulence effect is simulated using the power spectrum inversion method. Subsequently, the energy distribution on the target is modeled by considering the combination of multiple instantaneous on-target distributions, and the associated probability distribution is accounted for by incorporating the aiming and tracking error distribution. Applying principles from thermal physics, the on-target energy distribution is converted into an on-target temperature distribution, allowing for the calculation of the probability of damage, as mentioned in (1).

Directly calculating the on-spot energy density is difficult because it involves determining both the energy distribution and the area, which is complicated by the irregularity of the target. Instead, this process is simplified by computing the far-field energy distribution and the actual on-spot area using Monte Carlo methods and atmospheric turbulence inversion techniques, respectively.

It is assumed that the emitted laser is a Gaussian beam

$$I(x,y) = I_0 \exp\left(-2\left[\frac{x^2+y^2}{w^2}\right]\right), (x,y) \in \mathbf{R}^2 \tag{2}$$

where I_0 denotes the central peak light intensity, w denotes the beam waist and (x,y) denotes any point on the plane perpendicular to the direction of propagation.

If the effect of atmospheric turbulence on the refractive index of the media were to be studied using the Navier-Stokes equations, the computational inefficiency or impossibility would arise due to the need to solve 10^{16} to 10^{18} simultaneous differential equations. Therefore, the statistical model is used, which treats turbulence as a finite number of phase screens. A common method for constructing a phase screen involves using a turbulent refractive index spectrum and a complex Gaussian random number matrix to generate a phase space complex random field. The spatial distribution of the two-dimensional phase is then derived by an inverse Fourier transform. This method is known as power spectrum inversion.

Assuming that the atmospheric turbulence is isotropic and locally homogeneous, the refractive index spectral density function can be obtained based on the Kolmogorov atmospheric refractive

index structure function. The more optimized Von-Karman atmospheric refractive index spectral density function is as follows

$$\Phi_n(\kappa, z) = 0.033\, C_n^2(z) \left(\kappa_0^2 + \kappa^2\right)^{-11/6} e^{-\kappa/\kappa_m} \tag{3}$$

where κ is the number of waves in 3D space, and the range of values of κ is $\kappa_0 < \kappa < \kappa_m$. Here, $\kappa_0 = \frac{2\pi}{L_0}$ and $\kappa_m = \frac{5.92}{l_0}$, where l_0 and L_0 denote the inner and outer scales of turbulence, respectively. $C_n^2(z)$ is the Refractive Index Structure Parameter. It can be calculated using

$$C_n^2(z) = b \frac{K_H}{\epsilon^{\frac{1}{3}}} \left(\frac{\partial n}{\partial z}\right)^2$$

where b is equal to 3.2 and called the Obukhov-Corrsin constant, K_H is the turbulent exchange coefficient for heat diffusion, ϵ is the energy dissipation rate and $\frac{\partial n}{\partial z}$ is the vertical gradient of the index of refraction [9].
The atmospheric phase spectrum is given by

$$\Phi_\phi(\kappa_x, \kappa_y) = 2\pi k^2 \Phi_n(\kappa_x, \kappa_y). \tag{4}$$

$\Phi_n(\kappa_x, \kappa_y)$ is the power spectral density of refractive index fluctuations, describing how these fluctuations are distributed over spatial frequencies κ_x and κ_y. κ_x and κ_y are the spatial wavenumbers in the x- and y-directions, inversely related to the physical spatial scales [11].

The atmospheric phase screen function, $\phi_{sh}(x, y)$, is given by

$$\begin{aligned}\phi_{sh}(x, y) =& C \sum_{p=1}^{N_p} \sum_{m=0}^{N_x} \sum_{n=0}^{N_y} R(\kappa_x, \kappa_y) \Phi_\phi(\kappa_x, \kappa_y) \\ & \times e^{2\pi i \left(\frac{x}{3pD_x} + \frac{y}{3pD_y}\right)},\end{aligned} \tag{5}$$

where (x, y) denote the airspace coordinates, (κ_x, κ_y) denote the frequency domain coordinates, $R(\kappa_x, \kappa_y)$ denotes the random number that follows a Gaussian distribution. D_x and D_y represent characteristic spatial scales in the x- and y-directions, respectively. They describe the periodicity or spacing of phase fluctuations, possibly related to grid spacing or aperture size in optical systems, modulating the oscillatory phase shifts over these directions in wavefront propagation models.
The far-field spot energy distribution is given by

$$I_{yc}(x, y) = \left| \mathcal{F}^{-1} \left\{ H(f_x, f_y) \mathcal{F} \left\{ I(x, y) e^{i\phi_{sh}(x,y)} \right\} \right\} \right|^2 \tag{6}$$

where $\mathcal{F}$ and $\mathcal{F}^{-1}$ are the forward and inverse Fourier transforms, respectively, and $H(f_x, f_y)$ denotes the transfer function for free-space diffraction.

The laser weapon system is considered to be mounted at the origin of a coordinate system, with a vertically upward z-axis towards the sky. The target location, denoted by (x_t, y_t, z_t), is assumed to be the geometric center of a 3D structure. The laser beam, approximated as a cone with a half-angle θ_0, is aimed towards this point. The target's shape, simplified as a cylinder, is positioned horizontally around (x_t, y_t, z_t). This assumption is particularly applicable in scenarios involving missile interception using laser systems.

For Monte Carlo simulation, N points have been generated uniformly and randomly on the surface of the cylinder. Each point's angle with respect to the axis of the laser beam cone, denoted as α, is calculated; points where $0 \leq \alpha \leq \theta_0$ are considered within the cone. The number of such points, $N_{\text{in-cone}}$, is determined among the total points generated N.
The on-target spot area, denoted as S_{db}, is calculated using

$$S_{\text{db}} = \frac{N_{\text{in-cone}}}{N} \pi r l, \tag{7}$$

where r and l represent the dimensions of the target cylinder. This formula provides an effective measure of the focused energy on the target, considering the spatial distribution and alignment of the laser beam with the target's cylindrical shape.
Given the small half-angle of the laser beam, the intersection is approximated with the target surface as planar. Thus, it is assumed the irradiation occurs on a plane surface. Negligible power dissipation during laser transmission leads to

$$\iint\limits_{S_{yc}} I_{yc}(x,y)dxdy = \iint\limits_{S_{db}} I_{db},(x,y)dxdy \tag{8}$$

where $I_{\mathrm{yc}}(x,y)$ and $I_{\mathrm{db}}(x,y)$ are intensities at the far-field and on-target, respectively and S_{yc}, S_{db} are their respective areas. Assuming laser transmission along the z-direction and the x-y plane for surface spread, the spot center coordinates $(\bar{x},\bar{y})$ are determined by

$$(\bar{x},\bar{y}) = \left(\frac{\iint_S x\, I(x,y)\, dx\, dy}{\iint_S I(x,y)\, dx\, dy}, \frac{\iint_S y\, I(x,y)\, dx\, dy}{\iint_S I(x,y)\, dx\, dy} \right). \tag{9}$$

From the center $(\bar{x},\bar{y})$, a circle Ω of arbitrary radius is constructed within the surface S. Define the parameter η as

$$\eta = \frac{\sum_{(x,y)\in\Omega} I(x,y)}{\sum_{(x,y)\in S} I(x,y)}. \tag{10}$$

The radius of Ω is adjusted until η reaches 84%, using a suitable search algorithm such as binary search. For a Gaussian beam, approximately 84% of the total intensity is contained within one standard deviation of the distribution. Therefore, this value has been chosen. Note that any other value can also be chosen without affecting the qualitative aspects of results.
When aligning a laser beam to a target, mechanical vibrations cause tracking errors. The aiming error, $\hat{\phi}(x_c,y_c) = (u_x,u_y)$, measures deviation from the intended spot at (x_c,y_c).
Assuming Gaussian disturbances along x and y, the total tracking error $\hat{\phi}(x_s,y_s)$ is

$$\hat{\phi}(x_s,y_s) = \frac{1}{2\pi\sigma_d\sigma_f} \exp\left(-\rho \left[\frac{x_s^2}{\sigma_d^2} + \frac{y_s^2}{\sigma_f^2} \right] \right)$$

with σ_d and σ_f as standard deviations in x and y directions, respectively and ρ is the scaling factor that affects the decay the Gaussian function.
The combined aiming and tracking error $\hat{\phi}(x,y)$ is

$$\hat{\phi}(x,y) = \frac{1}{2\pi\sigma_x\sigma_y} \exp\left(-\frac{1}{2} \left[\frac{(x-u_x)^2}{\sigma_x^2} + \frac{(y-u_y)^2}{\sigma_y^2} \right] \right), \tag{11}$$

where (x,y) are surface coordinates.
Let (x_i,y_i) denote the instantaneous location of the center of the on-target spot, and the probability that spot (x_i,y_i) will be achieved during a time interval Δt is given by $\hat{\phi}(x_i,y_i)$. The total incident energy density around the target point (x,y) is calculated using the superposition of all these instantaneous spots during the laser working period. The formula for the calculation is

$$E_{\mathrm{inc}}(x,y) = \sum_{i=1}^{N} I(x_i,y_i)\Delta t, \tag{12}$$

where (x,y) is the target point, $E_{\mathrm{inc}}(x,y)$ is the on-spot energy density around the target point and $I(x_i,y_i)$ denotes the incident intensity on the instantaneous center. We generate deviations with the help of Equation (12) and add them to the target point (x,y) to obtain the instantaneous center (x_i,y_i). We generate N such points for one simulation to compute the on-spot energy density. Many simulations are conducted to obtain a statistical histogram. By normalizing this

histogram, we derive a probability density function (PDF) of the energy distribution.
The energy distribution obtained above is converted to the temperature distribution under the assumption that the wall thickness is δ, and the laser propagates in the z-direction. This simplifies the calculation greatly as

$$\frac{1}{\kappa}\frac{\partial T}{\partial t} = \nabla^2 T = \frac{\partial^2 T}{\partial z^2} \tag{13}$$

where t is time, T is temperature, and $\kappa = \frac{k}{\rho c}$ where k is thermal conductivity, ρ is density of material, and c is specific heat. Since the propagation of laser is assumed to be in the z direction so the heat distributions along the x and y directions can be neglected i.e., $\frac{\partial^2 T}{\partial x^2} = 0$, $\frac{\partial^2 T}{\partial y^2} = 0$. The boundary conditions are

$$T(x,y,z,0) = T_0, \quad -k\frac{\partial T}{\partial z}\bigg|_{z=0} = \frac{AE_{\text{inc}}}{t}, \quad k\frac{\partial T}{\partial z}\bigg|_{z=\delta} = 0. \tag{14}$$

Solving these, we obtain:

$$T(x,y,z,t) = T_0 + \frac{AE_{\text{inc}}}{t}\left(\frac{\kappa t}{k\delta} + \frac{\delta}{k}\frac{3(\delta - z)^2 - \delta^2}{6\delta^2} - \zeta\right), \tag{15}$$

where ζ is

$$\zeta = \frac{2\delta}{\pi^2 k}\sum_{n=1}^{\infty}(-1)^n \frac{e^{-k\pi^2 n^2 t/\delta^2}\cos\left(\frac{n\pi(\delta - z)}{\delta}\right)}{n^2}.$$

Once the distribution for the incident energy density E_{inc} is obtained from Equation (12), it can be substituted into Equation (15) to derive the temperature distribution. The surface is then discretized into a grid of appropriate size, which is determined by the desired accuracy of the calculations. The probability of damage can subsequently be calculated using Equation (1). This is achieved by counting the grid squares where the temperature exceeds the threshold temperature T_D. The probability density function (PDF) of the temperature distribution is computed by iterating over each square in the grid, noting the temperature range corresponding to each square, and populating a histogram based on these observations. Finally, a fitting procedure is applied to obtain a smooth PDF from the histogram data.
To clarify things, the following assumptions for the model have been considered throughout this section.

- Precise energy distribution requirement and effect of the target surface irradiation have not been considered as it involves detailed material modeling, especially for composite materials.
- The laze time for hard kill is kept variable as per requirements.
- Laser beam are ideal Gaussian intensity profile.
- Kolmogorov atmospheric turbulence theory is used to develop the effects of turbulence on laser.
- Visibility range is assumed to be indefinite.

3. SIMULATION RESULTS

In this section, we list the results that we obtained from the simulation of the model, as outlined in Section 2.

3.1. Laser Beam Profiles

Figure 1 shows that the beam profiles at different distances show the effect of turbulence in the atmosphere. Figure 2 exhibits a typical phase screen that models the turbulence effects of the atmosphere on the laser by introducing phase shifts. Figure 3 shows typical Monte Carlo simulation for calculating on-spot area, with 10,000 points generated on the half-cylinder. Points within the laser cone are marked in red.

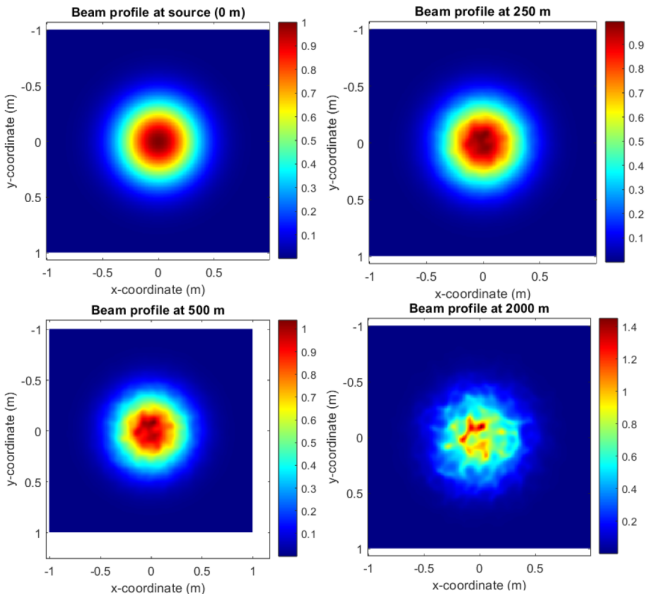

Figure 1: *The beam profiles at different distances.*

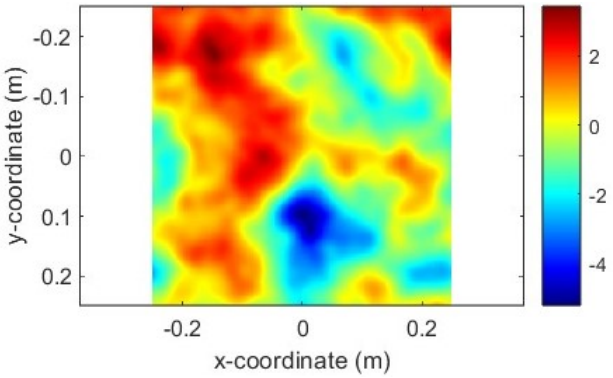

Figure 2: *Phase screen with the turbulence effects of the atmosphere.*

3.2. Effect of Distance on Damage Probability

The beam is supposed to show an exponential decay of the power with the distance $exp(-z)$. The simulation results for the same is shown in Figure 4.

3.3. Effect of Turbulence on the Damage Probability

The effect of turbulence on the damage probability is simulated by changing the value of the atmosphere™s inner and outer scale values and is shown in Figure 5. As the x-axis increases, atmospheric turbulence decreases, while the y-axis represents the damage probability of aluminum exposed to a 50 kW laser at a distance of 1 km.

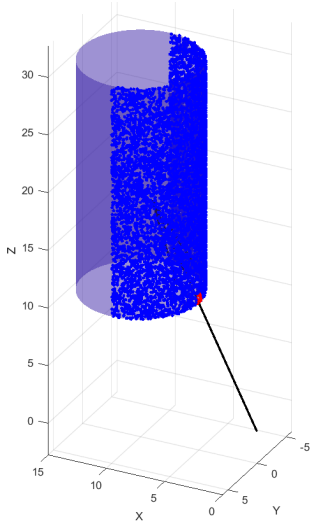

Figure 3: *Monte Carlo simulation results*

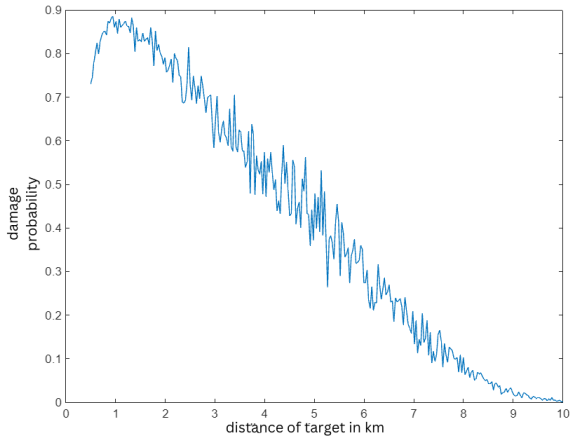

Figure 4: *Damage probability versus distance*

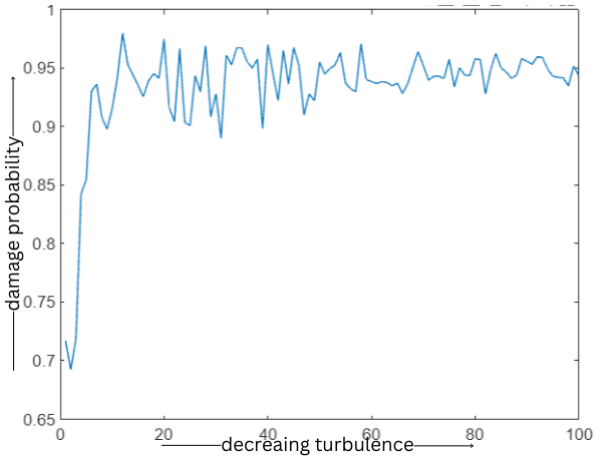

Figure 5: *Damage probability versus turbulence*

3.4. Minimum Power Required for Different Materials

The thermal conductivity is in W/cmK, the density is in g/cm3, specific heat is in J/gK, and the melting point is in degrees Celcius. The power is reported in the Table if the damage probability

calculated from the model turns out to be around 0.95 for moderate turbulence. The results of the simulation for few selected metals can be seen in Table 1 and the rest can be accessed here. The plots presented in Figures 6, 7, 8, and 9 illustrate the minimum laser power required (in kW) for a 2-second irradiation, as derived from the data in Table 1.

- Figure 6 displays the relationship between laser power and the density of the target material.
- Figure 7 illustrates how the required laser power varies with the melting point of the material.
- Figure 8 shows the correlation between laser power and the specific heat of the target.
- Figure 9 highlights the dependence of laser power on the thermal conductivity of the material.

These figures collectively provide insights into how various material properties influence the required laser power for effective thermal damage.

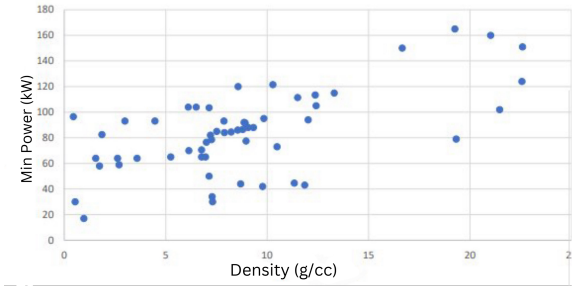

Figure 6: *Variation of the power of the laser versus the density of the target material*

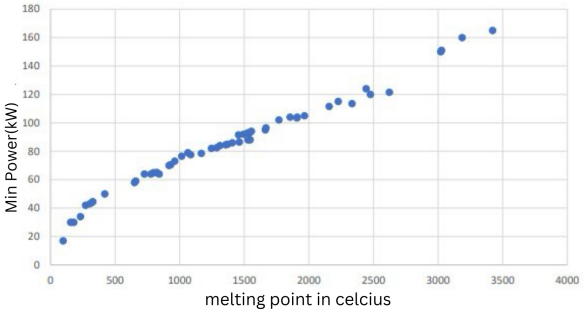

Figure 7: *Variation of the power of the laser versus the melting point of the target material*

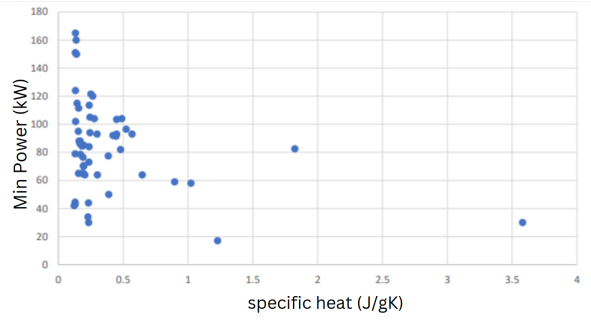

Figure 8: *Variation of the power of the laser versus the specific heat of the target material*

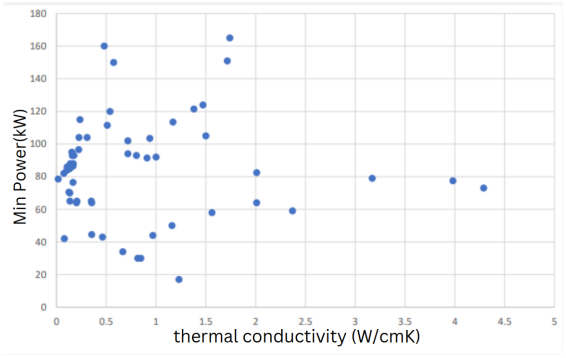

Figure 9: *Variation of the power of the laser versus the thermal conductivity of the material.*

From the plots, it can be concluded that the melting point is the most sensitive parameter, followed by the density of the material. The thermal conductivity and the specific heat of the material are very less sensitive parameters.

Table 1: *Properties of Various Elements*

Element	Thermal Conductivity	Density	Specific Heat	Melting Point	Min Power of Laser
Li	0.847	0.534	3.58	180.5	30
Be	2.01	1.85	1.824	1287	82.5
Mg	1.56	1.738	1.023	650	58
Al	2.37	2.7	0.897	660.32	59
Ca	2.01	1.55	0.647	842	64
Cr	0.937	7.14	0.449	1907	103.5
Mn	0.074	7.21	0.479	1246	82
Fe	0.803	7.874	0.449	1538	93
Co	1	8.86	0.421	1495	92
Ni	0.909	8.912	0.444	1455	91.5
Cu	3.98	8.96	0.385	1084.62	77.5
Zn	1.16	7.14	0.388	419.73	50
Ag	4.29	10.49	0.235	961.78	73
W	1.74	19.25	0.132	3422	165

4. CASE STUDY: ATTACKING A DRONE

We assume that the drone is made up of composite carbon material. The attack's parameters and results are mentioned in Table 2. The results indicate a 93.6% probability that the drone will sustain damage. The simulation findings are illustrated in Figures 10, 11, and 12. The left panel of Figure 10 displays the energy distribution at a distance (far-spot), while the right panel presents the energy distribution at the targeted location (on-spot). Both images are annotated with an 84% irradiation circle.

5. PSEUDO CODE

In this section, the pseudo codes are provided which have been used to develop the simulation to generate the results. Please refer, pseudo codes 1, 2, 3, 4, 5, 6.

6. CONCLUSIONS AND FUTURE WORKS

This study provides an extensive probability analysis of a thermal laser weapon system intended to destroy drones and other aerial threats. An efficient model that takes into account the effects

Pseudo Code 1 MONTE_CARLO_AREA_CALCULATION

function MONTE_CARLO_AREA_CALCULATION(r, l, xc, yc, zc, N_points, α)
  $red\_points \leftarrow 0$
  $laser\_dir \leftarrow [xc, yc, zc] - [0, 0, 0]$
  $laser\_dir \leftarrow laser\_dir / \|\textsc{Norm}(laser\_dir)\|$
  $z \leftarrow zc - \frac{l}{2} + l \cdot \textsc{Random}(N\_points, 1)$
  $\theta \leftarrow -\frac{\pi}{2} + \pi \cdot \textsc{Random}(N\_points, 1)$
  $x\_points \leftarrow xc - r \cdot \cos(\theta)$
  $y\_points \leftarrow yc - r \cdot \sin(\theta)$
  for $i \leftarrow 1$ **to** N_points **do**
    $point \leftarrow [x\_points[i], y\_points[i], z[i]]$
    $norm\_point \leftarrow \|\textsc{Norm}(point)\|$
    $cross\_product \leftarrow \|\textsc{Cross\_Product}(laser\_dir, point)\|$
    $angle \leftarrow \left|\textsc{Asin}\left(\frac{cross\_product}{norm\_point}\right)\right|$
    if $angle < \alpha$ **then**
      $red\_points \leftarrow red\_points + 1$
    end if
  end for
  $S\_onspot \leftarrow \left(\frac{red\_points}{N\_points}\right) \cdot \pi \cdot r \cdot l$
  return S_onspot
end function

Pseudo Code 2 FT_SH_PHASE_SCREEN

function FT_SH_PHASE_SCREEN(r_0, N, δ, L_0, l_0)
  $D \leftarrow N \cdot \delta$
  $phz\_hi \leftarrow$ FT_PHASE_SCREEN(r_0, N, δ, L_0, l_0)
  $(x, y) \leftarrow \textsc{Create\_Spatial\_Grid}(N, \delta)$
  $phz\_lo \leftarrow \textsc{Zero\_Matrix}(N, N)$
  for $p \leftarrow 1$ **to** 3 **do**
    $del\_f \leftarrow \frac{1}{3^p \cdot D}$
    $(f_x, f_y) \leftarrow \textsc{Create\_Frequency\_Grid}(del\_f)$
    $(angle, f) \leftarrow \textsc{Convert\_To\_Polar}(f_x, f_y)$
    $f_m \leftarrow \frac{5.92}{l_0 \cdot (2\pi)}$
    $f_0 \leftarrow \frac{1}{L_0}$
    $PSD\_phi \leftarrow 0.023 \cdot r_0^{-5/3} \cdot \exp\left(-\left(\frac{f}{f_m}\right)^2\right) / (f^2 + f0^2)^{11/6}$
    $PSD\_phi[2][2] \leftarrow 0$
    $cn \leftarrow (\textsc{Random\_Normal\_Matrix}(3,3) + 1i \cdot \textsc{Random\_Normal\_Matrix}(3,3)) \cdot \sqrt{PSD\_phi} \cdot del\_f$
    $SH \leftarrow \textsc{Zero\_Matrix}(N, N)$
    for $ii \leftarrow 1$ **to** 9 **do**
      $SH \leftarrow SH + cn[ii] \cdot \exp\left(1i \cdot 2\pi \cdot (f_x[ii] \cdot x + f_y[ii] \cdot y)\right)$
    end for
    $phz\_lo \leftarrow phz\_lo + SH$
  end for
  $phz\_lo \leftarrow \textsc{Real}(phz\_lo) - \textsc{Mean}(\textsc{Real}(phz\_lo))$
  return (phz_lo, phz_hi)
end function

Pseudo Code 3 FT_PHASE_SCREEN

function FT_PHASE_SCREEN(r_0, N, δ, L_0, l_0)
  $D \leftarrow N \cdot \delta$
  $del\_f \leftarrow \frac{1}{D}$
  $f_x \leftarrow$ CREATE_ARRAY($-\frac{N}{2}$ **to** $\frac{N}{2} - 1$) $\cdot del\_f$
  $(f_x, f_y) \leftarrow$ MESHGRID(f_x, f_y)
  $f \leftarrow \sqrt{f_x^2 + f_y^2}$
  $f_m \leftarrow \frac{5.92}{l_0 \cdot (2\pi)}$
  $f_0 \leftarrow \frac{1}{L_0}$
  $PSD\_phi \leftarrow 0.023 \cdot r_0^{-5/3} \cdot \exp\left(-\left(\frac{f}{f_m}\right)^2\right) / (f^2 + f_0^2)^{11/6}$
  $PSD\_phi[\frac{N}{2}][\frac{N}{2}] \leftarrow 0$
  $random\_real \leftarrow Random\_Normal\_Matrix(N, N)$
  $random\_imag \leftarrow Random\_Normal\_Matrix(N, N)$
  $cn \leftarrow (random\_real + i \cdot random\_imag) \cdot \sqrt{PSD\_phi} \cdot del\_f$
  $phz\_hi \leftarrow Inverse\_FFT2(Shift\_FFT(cn)$, 'symmetric') $.(N \cdot del\_f)^2$

  return phz_hi
end function

Pseudo Code 4 PROPAGATE_BEAM

function PROPAGATE_BEAM(E_{in}, λ, dz, δ)
  $N \leftarrow$ SIZE(E_in, 1)
  $fx \leftarrow$ CREATE_SPATIAL_FREQUENCIES(N, δ)
  $H \leftarrow$ CALCULATE_TRANSFER_FUNCTION(fx, λ, dz)
  $E\_in\_ft \leftarrow$ FOURIER_TRANSFORM(E_{in})
  $E\_out\_ft \leftarrow E_{in\_ft} \cdot H$
  $E\_out \leftarrow$ INVERSE_FOURIER_TRANSFORM(E_out_ft)
  return E_out
end function

Pseudo Code 5 DRIVER CODE

function ON_SPOT_ENERGY(*therma*, *density*, *specific*, *melt*, *amp*)
Set parameters
D // Length of one side of square phase screen [m]
$r0$ // Coherence diameter [m]
N // Number of grid points per side
$L0$ // Outer scale [m]
$l0$ // Inner scale [m]
$\delta \leftarrow \frac{D}{N}$ // Grid spacing [m]
$amplitude \leftarrow amp$ // Amplitude in kilowatt
λ // Wavelength [m]
$w0$ // Beam waist [m]
L // Single propagation distance [m]
$k \leftarrow therma \cdot 100$ // Thermal conductivity [W/(m*K)]
$\rho \leftarrow density$ // Density [g/cm^3]
$c \leftarrow specific$ // Specific heat [$J/(g*K)$]
$\delta\_material$ // Wall thickness [m]
$T0$ // Initial temperature [C]
A // Area coefficient (arbitrary units)
TD // Threshold temperature for damage [C]
$time\_step$ // Time step for temperature calculation [s]
Calculate thermal diffusivity
$\kappa \leftarrow \frac{k}{\rho \cdot c}$ // Thermal diffusivity [m^2/s]
Create the phase screens
$(phz\_lo, phz\_hi) \leftarrow$ GENERATE_PHASE_SCREENS($r0$, N, δ, $L0$, $l0$)
$phz \leftarrow phz\_lo + phz\_hi$
Create spatial grid
$x \leftarrow$ GENERATE_GRID($-\frac{N}{2}$, $\frac{N}{2} - 1$, δ)
$y \leftarrow x$
$(X, Y) \leftarrow$ MESHGRID(x, y)
Initial Gaussian beam profile with amplitude factor
$E0 \leftarrow amplitude \cdot \exp\left(-\frac{X^2+Y^2}{w0^2}\right)$
Number of phase screens and distance between screens
$M \leftarrow ...$
$dz \leftarrow \frac{L}{M}$
Propagate the beam through the phase screens
$E \leftarrow E0$
for $m \leftarrow 1$ **to** M **do**
Apply the phase screen
$E \leftarrow E \cdot \exp(i \cdot phz)$
Propagate to the next screen
$E \leftarrow$ PROPAGATE_BEAM(E, λ, dz, δ)
end for
Calculate the instantaneous center of the intensity distribution
$I \leftarrow |E|^2$
$x\_bar \leftarrow \frac{\sum\sum(X \cdot I)}{\sum\sum I}$
$y\_bar \leftarrow \frac{\sum\sum(Y \cdot I)}{\sum\sum I}$
end function

Pseudo Code 6 DRIVER CODE CONTINUE

Monte Carlo simulation for area calculation
$total\_energy\_distribution \leftarrow 0$
for each simulation **from** 1 **to** num_simulations **do**
Generate a new center using a 2D Gaussian distribution
$new\_center \leftarrow$ SAMPLE_FROM_2D_GAUSSIAN($[x\_bar, y\_bar]$, $[variance, variance]$)
$x\_new \leftarrow new\_center.x$
$y\_new \leftarrow new\_center.y$
Generate the new intensity distribution centered at (*x_new*, *y_new*)
$E\_shifted \leftarrow amplitude \cdot \exp\left(-\frac{(X-x\_new)^2+(Y-y\_new)^2}{w0^2}\right) \cdot \exp(i \cdot phz)$
Propagate the beam through the phase screens
for each propagation step **from** 1 **to** M **do**
$E\_shifted \leftarrow$ PROPAGATE_BEAM($E\_shifted$, λ, dz, δ)
end for
Calculate intensity for shifted beam
$I\_shifted \leftarrow |E\_shifted|^2$
Calculate new center and radius for shifted beam using the formula given in the text
$(x\_bar\_shifted, y\_bar\_shifted) \leftarrow$ CALCULATE_CENTER($I\_shifted$)
$final\_radius\_shifted \leftarrow$ CALCULATE_FINAL_RADIUS(X, Y, $I\_shifted$, $x\_bar\_shifted$, $y\_bar\_shifted$)
Calculate the area of the far-field spot with 84% energy
$S\_farspot\_84 \leftarrow \pi \cdot final\_radius\_shifted^2$
Calculate the on-spot intensity
$I\_onspot \leftarrow I\_shifted \cdot \frac{S\_farspot\_84}{S\_onspot}$
Accumulate the energy distribution
$total\_energy\_distribution \leftarrow total\_energy\_distribution + I\_onspot \cdot delta\_t$
end for
Normalize the accumulated energy distribution
$total\_energy\_distribution \leftarrow total\_energy\_distribution / (num\_simulations \cdot delta\_t)$
Calculate the temperature distribution using the formula mentioned in the text
$T \leftarrow$ CALCULATE_TEMPERATURE($total\_energy\_distribution$, $T0$, A, $time\_step$, κ, $\delta\_material$, L, k)
Calculate the probability of damage
$p\_damage \leftarrow \frac{\sum(T(:)>TD)}{\text{LENGTH}(T)}$
PRINT('Probability of Damage: ', p_damage)

Table 2: *Material and Laser Parameters*

Parameter	Value	Parameter	Value
Material	Carbon Fiber	Thermal Conductivity	2 W/cmK
Density	2 g/cm^3	Specific Heat	1 J/gK
Thickness	1 cm	Melting Point	3650 °C
Outer Scale	15 m	Inner Scale	0.18 m
Laze Time	20 seconds	Power of the Laser	18 kW
Distance	1 km	Initial Temperature	50 °C

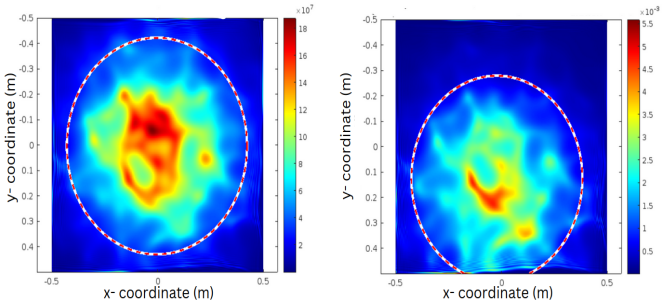

Figure 10: *Far-spot energy distribution (left) and the on-spot energy distribution (right)*

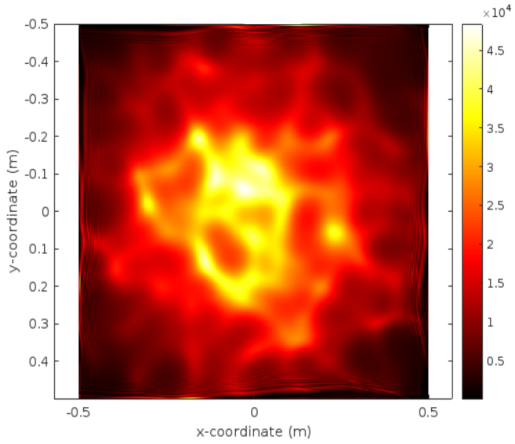

Figure 11: *Temperature distribution*

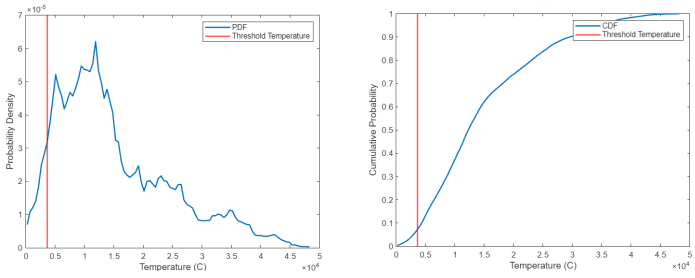

Figure 12: *The PDF and CDF of the temperature distribution function*

of atmospheric turbulence on laser propagation, the energy distribution on the target, and the thermal reaction of the target material was created. The chance of damage occurring from

persistent laser irradiation has been derived by simplifying complex interactions through the use of statistical methods and Monte Carlo simulations. The findings of the simulation suggest that the efficiency of a thermal laser weapon system is highly dependent on the target's material qualities, the laser system's accuracy, and the air conditions.

Future research could enhance this analysis by incorporating additional factors affecting laser performance, such as scintillation, aerosol scattering, absorption, humidity, and thermal blooming. Including these atmospheric effects is crucial for practical applications. Additionally, dynamic target analyses could refine and validate the model for robustness in diverse operational scenarios.

References

[1] Abunada, A.H., Osman, A.Y., Khandakar, A., Chowdhury, M.E.H., Khattab, T., Touati, F.: Design and implementation of a rf based anti-drone system. In: 2020 IEEE International Conference on Informatics, IoT, and Enabling Technologies (ICIoT). pp. 35–42. Doha, Qatar (Feb 2020)

[2] L. Liao, X.H., Xie, F.: Development status and operation analysis of laser weapon in anti-drone warfare. In: 2023 IEEE International Conference on Unmanned Systems (ICUS). pp. 305–310. Hefei, China (Oct 2023)

[3] Liu, L., Xu, C., Zheng, C., Cai, S., Wang, C., Guo, J.: Vulnerability assessment of uav engine to laser based on improved shotline method. Defence Technology **33**, 588–600 (2023)

[4] Lyu, C., Zhan, R.: Global analysis of active defense technologies for unmanned aerial vehicle. IEEE Aerospace and Electronic Systems Magazine **30**(1), 6–31 (2022)

[5] Mengzhen, Z., Xia, C., Xu, L., Chaoyong, T., Wei, L.: Situation and key technology of tactical laser anti-uav. Infrared Laser Eng **50**(7), 20200230–1 (2021)

[6] Perram, G.P., Marciniak, M.A., Goda, M.: High-energy laser weapons: technology overview. Laser Technologies for Defense and Security **5414**, 1–25 (2004)

[7] RE, B.: The fundamentals of aircraft combat survivability: analysis and design. 2th ed. Reston: American Institute of Aeronautics and Astronautics (1985)

[8] Steinvall, O.: The potential role of lasers in combating uavs, part 1: detection, tracking, and recognition of uavs. In Electro-Optical and Infrared Systems: Technology and Applications XVIII and Electro-Optical Remote Sensing XV **11866**, 174–185 (2021)

[9] Tunick, A.D.: The refractive index structure parameter/atmospheric optical turbulence model: Cn2. Tech. Rep. ARL-TR-1615, Army Research Laboratory, Adelphi, MD (Apr 1998)

[10] Voorst, B.R.V.: Counter drone system. U.S. Patent 15 443 143 **14** (2017)

[11] Wang, F., Du, W., Yuan, Q., Liu, D., Feng, S.: A survey of structure of atmospheric turbulence in atmosphere and related turbulent effects. Atmosphere **12**(12) (2021). https://doi.org/10.3390/atmos12121608, https://www.mdpi.com/2073-4433/12/12/1608

[12] Wang, P., Luo, J., Tang, J., Qin, Y., Cui, J., Zhang, L.: Progress and prospects of anti-drone radar detection technology. In: 2021 CIE International Conference on Radar (Radar). pp. 2331–2334. Hainan, China (Dec 2021)

[13] Zhao, S., Xie, R., Wan, J.: Design of anti-drone laser weapon systems. In: High-Power Lasers and Applications XI. pp. 24–30. Hefei, China (Oct 2023)